11-2009

# Linker-Free Modification Of TiO2 Nanorods With PbSe Nanocrystals

Krishna P. Acharya

Taiwo R. Alabi

Nicholas Schmall

Nishshanka N. Hewa-Kasakarage

Maria Kirsanova

*See next page for additional authors*

# Linker-Free Modification of $TiO_2$ Nanorods with PbSe Nanocrystals

**Krishna P. Acharya, Taiwo R. Alabi, Nicholas Schmall, Nishshanka N. Hewa-Kasakarage, Maria Kirsanova, Alexander Nemchinov, Elena Khon, and Mikhail Zamkov***

*The Center for Photochemical Sciences and Department of Physics, Bowling Green State University, Bowling Green, Ohio 43403*

*Received: July 30, 2009; Revised Manuscript Received: September 18, 2009*

We report on a colloidal synthesis of PbSe/$TiO_2$ heterostructures, comprising small-diameter PbSe nanocrystals epitaxially grown onto the surface of $TiO_2$ nanorods. The deposition of lead selenide onto prefabricated $TiO_2$ nanocrystals proceeds via formation of a thin PbSe shell that subsequently breaks into sub-2-nm islands. Additional precursor injections are then used to increase the size of PbSe nanocrystals up to 5 nm. In the case of small-size PbSe, a 2.1-ns transfer of photoinduced carriers into $TiO_2$ domain was evidenced through quenching of the PbSe band gap emission. Overall, the present synthesis demonstrates a colloidal approach to all-inorganic modification of $TiO_2$ surfaces with semiconductor nanocrystals, which provides a viable alternative to a more common supramolecular assembly of nanocrystal-oxide composites.

## 1. Introduction

Titanium dioxide is an important photovoltaic and photocatalytic material,[1] which utilization in dye-sensitized solar cells,[2] and hydrogen production[3] is encouraged by its low fabrication costs and minimal environmental hazards. Efficient harvesting of solar radiation within $TiO_2$ generally requires extending its absorption range into the visible and near-infrared range by introducing an appropriate sensitizer that engages in an electron-transfer reaction with an oxide material upon receiving a photon of light. To date, the most common strategy for the sensitization of $TiO_2$ involves modification of its surface with organic-based transition-metal complexes, such as porphyrins[4] or Ru complexes.[2] However, incorporation of semiconductor nanocrystals (NC) as sensitizers is now being actively explored[5–20] because of a number of advantages offered by inorganic NCs, including wider absorption profile, superior resistance to photobleaching, and continuous tunability of NC conduction levels.

As shown by recent reports, successful modification of anatase $TiO_2$ or amorphous $TiO_x$ with colloidal CdSe,[12] InAs,[21] PbSe,[22] and PbS[23] NCs can be achieved in a reproducible manner, leading to heterostructures that exhibit photoinduced charge separation. In these works, however, deposition of colloidal nanocrystals onto the oxide material still relies on organic linkers or nonepitaxial contacts with NC ligands,[22] which makes it difficult to extract photoinduced carriers from NC domains, leading to the decrease in electron-transfer rates and carrier trapping at hybrid interfaces. For instance, surprisingly slow photoinduced electron transfer has been reported in organically coupled PbS−$TiO_2$ systems.[23] To avoid these problems, several groups have attempted in situ growth of CdS[24–26] NCs onto mesoporous $TiO_2$ films in ionic solutions. Although the observation of the 2−3-fold increase in the solar conversion efficiency of such films was encouraging, the quality and size distribution of NCs fabricated using this approach were inferior to those synthesized through colloidal techniques, making it difficult to control the relative positions of electron energy levels in a donor−acceptor system.

Here we demonstrate a colloidal route to the synthesis of PbSe/$TiO_2$ hetero-nanocrystals (HNCs), comprising 2−5 nm PbSe NCs grown directly on the surface of $TiO_2$ nanorods (NRs). As a main benefit of colloidal injection techniques, the present approach allows for a controlled adjustment of the sensitizer electronic levels via tuning the average NC diameter during synthesis, which is critical for the experimental realization of a desired type II (staggered) offset of donor and acceptor conduction band edges. Moreover, formation of a near-epitaxial interface between PbSe and $TiO_2$ domains enables a rapid injection of photoinduced carriers into the oxide material, which was demonstrated via a 50-fold increase in the photoinduced electron-transfer rate between PbSe and $TiO_2$ domains, as compared to organically linked lead chalcogenide−$TiO_2$ assemblies.[23]

## 2. Experimental Section

**2.1. Chemicals.** 1-Octadecene (ODE, 90%, Aldrich), oleylamine (OLAM, 70%, Aldrich), oleic acid (OA, 90%, Aldrich), titanium tetrachloride ($TiCl_4$, 99.9%, Aldrich), lead(II) oxide powder (PbO, 99.999%, Aldrich), selenium powder (Se, 99.5%, Acros), sulfur (99.999%, Acros), ODE(tech., 90%, Aldrich), tri-*n*-octylphosphine oxide (TOPO, 99%, Aldrich), selenium (99.5+%, Acros), hexane (anhydrous, 95%, Aldrich), methanol (anhydrous, EMD), toluene (anhydrous, 99.8%, Aldrich), and chloroform (anhydrous, 99+%, Aldrich) were all used as received without any further purification. All reactions were performed under an argon atmosphere using the standard Schlenk technique.

**2.2. Preparation of Injection Precursors.** The lead precursor was prepared by dissolving 0.45 g (2.0 mmol) of lead oxide in a mixture of 1.6 g of OA and 4 g of ODE by heating the flask to 200 °C for 30 min. Prior to the injection the temperature of the Pb solution was lowered to 140 °C. One molar TOP−Se solution was prepared by dissolving 0.21 g of Se in 2.7 mL of TOP at room temperature and heated up to 100 °C prior to injection. Two different approaches were used to prepare a sulfur stock solution (see Supporting Information for PbS/$TiO_2$ het-

* To whom correspondence should be addressed. E-mail: zamkovm@bgsu.edu.

10.1021/jp907321h CCC: $40.75 
Published on Web 10/21/2009

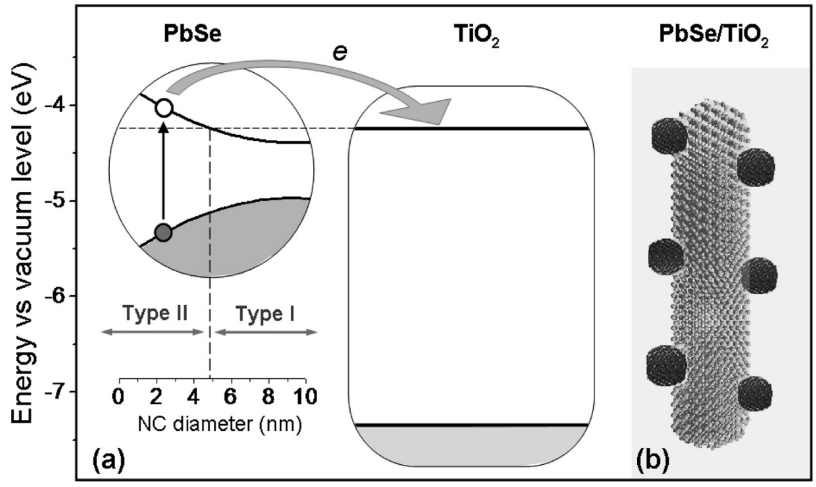


**Figure 1.** (a) Size-dependent energies of 1S(e) electronic levels for PbSe NCs and $TiO_2$ nanorods. Photoinduced electron transfer from PbSe to $TiO_2$ is energetically allowed if the PbSe diameter is less than 5 nm. (b) Schematic representation of the Volmer−Weber regime of heteroepitaxial growth, where the energy of the PbSe/$TiO_2$ interface is reduced through the formation of island-like features.

erostructures). As a low-reactive precursor, 0.04 g of sulfur was combined with 3 mL of ODE and subsequently heated to 200 °C to form a clear solution. Prior to the injection, the mixture was cooled down to room temperature. As a more reactive source of sulfur, 0.3 mL of hexamethyldisilthiane was combined with 3 mL of degassed ODE at room temperature.

**2.3. Synthesis of PbSe/$TiO_2$ Heterostructures.** A one-pot synthesis of PbSe/$TiO_2$ proceeded via the initial growth of $TiO_2$ nanorods onto which PbSe NCs were subsequently grown by injecting lead selenide precursors at lower temperature. Typically, 6.5 mmol of OLAM and 1 mmol of OLAC were mixed in a three-neck flask and degassed using a mechanical vacuum pump at 120 °C for 30 min. The mixture was subsequently switched to argon and 1 mmol of $TiCl_4$ was injected into the flask at 40 °C. The reaction flask was then heated to 300 °C and maintained at that temperature for 30 min. To initiate the growth of PbSe NCs, the temperature of the reaction mixture was lowered to 190 °C and warm precursors of Pb ($T = 100$ °C) and Se ($T = 80$ °C) were injected simultaneously. Typically 3−5 mL of lead and 1.3−3 mL of Se stock solutions were used during the first injection. The subsequent injection(s) were made 4 min after the first (or previous). Grown nanostructures were purified using several toluene/ethanol extractions.

**2.4. Characterization.** UV−vis absorption and photoluminescence spectra were recorded using a CARY 50 Scan spectrophotometer and a Jobin Yvon Fluorolog FL3-11 fluorescence spectrophotometer. High-resolution transmission electron microscopy measurements were carried out using a JEOL 3011UHR operated at 300 kV. Specimens were prepared by depositing a drop of nanocrystal hexane solution onto a Formvar-coated copper grid and allowing it dry in air. X-ray powder diffraction measurements were carried out on a Scintag XDS-2000 X-ray powder diffractometer. Energy-dispersive X-ray (EDX) emission spectra were measured using an EDAX X-ray detector located inside a scanning electron microscope. The electron beam was accelerated at 20 kV.

**2.5. Fluorescence Lifetime Measurements.** FL lifetime measurements were performed using a time-correlated single-photon counting setup utilizing a SPC-630 single-photon counting PCI card (Becker & Hickle CmbH), picosecond diode laser operating at 400 nm, as an excitation source (Picoquant), and an id50 avalanche photodiode (Quantique). The repletion rate of the laser was chosen to allow for a 1000 ns time window, whereas the pulse fluence was adjusted to produce about 1 emission photon per 100 excitation pulses (excitation power was 100 $\mu$W).

## 3. Results and Discussion

In the case of colloidal heterostructures, the type of inorganic interface that forms at the boundary of the two material domains is determined by the relationship between the total surface energy of the composite nanoparticle and the solid−solid interfacial energy related to the mismatch-induced strain between the two lattices. If the interfacial strain exceeds the surface tension of either material, such structure may undergo a spatial rearrangement that eliminates some of the interfacial region by increasing the overall surface area.[27] This scenario is clearly observed for PbSe/$TiO_2$ heterostructures, where a large lattice mismatch of either 6.7% or 18% corresponding to merging of 010 and 110 (Figure 3b) or 001 and 100 faces of anatase $TiO_2$ and rock-salt PbSe crystal lattices leads to the Volmer−Weber growth of the PbSe material, characterized by the formation of small PbSe islands throughout the surface of $TiO_2$ (Figure 1b). One potential benefit associated with such a growth mode is the possibility of increasing the optical extinction coefficient of these nanoparticles by sintering several PbSe sensitizers per single $TiO_2$ NR. Since the light-absorption cross section of 2 nm PbSe NCs is generally small ($\sim 2 \times 10^{-15}$ cm$^2$, $\lambda = 400$),[28] the maximum number of electron−hole pairs generated in a single PbSe/$TiO_2$ structure, under ambient illumination (photon flux $\approx 3 \times 10^{21}$ m$^{-2}$s) is less than 1, which is not expected to produce nonlinear charging effects.[29] As a result, increasing the number of PbSe sites in PbSe/$TiO_2$ heterostructures should result in a linear increase of the power conversion efficiency in NC-sensitized solar cells.

Another benefit of the Volmer−Weber growth regime is the thermodynamically stable formation of small-diameter PbSe NCs, which is critical for the realization of a type II heterojunction between PbSe and $TiO_2$ materials. Indeed, according to the energy diagram of electronic states in PbSe NCs (Figure 1a), calculated from electron injection studies[30,31] and empirical scaling of band edge absorption, the transfer of photoinduced electrons from PbSe to $TiO_2$ is energetically permissible only if the size of PbSe is less than 5 nm.

Schematics of the one-pot approach to the synthesis of PbSe/$TiO_2$ HNCs are illustrated in Figure 2a. Growth of $TiO_2$ NRs

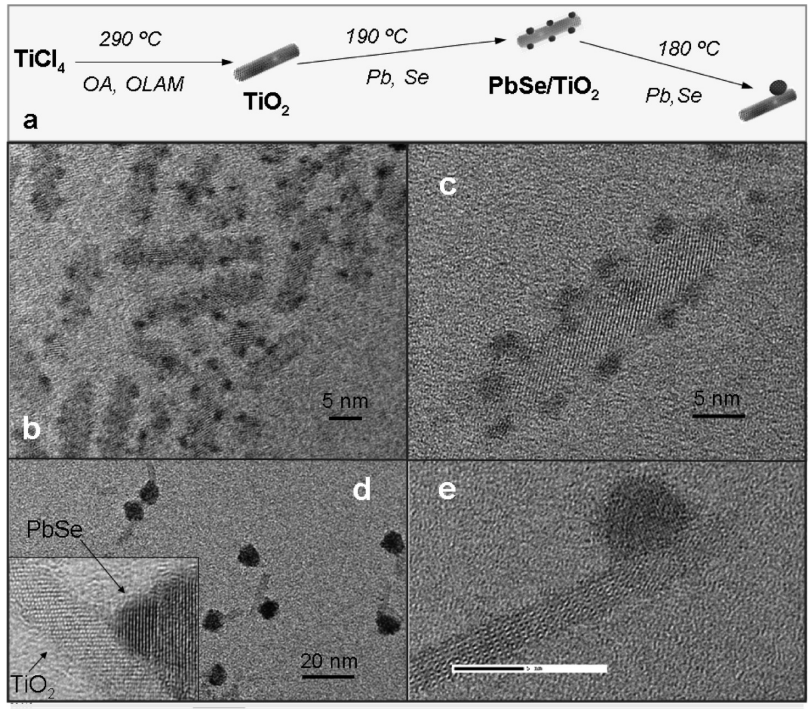


**Figure 2.** (a) Schematics of the PbSe/$TiO_2$ synthesis. (b−e) Transmission electron microscopy images of PbSe/$TiO_2$ HNCs that form after the initial (b,c) and secondary (d,e) injections of Pb and Se precursors.

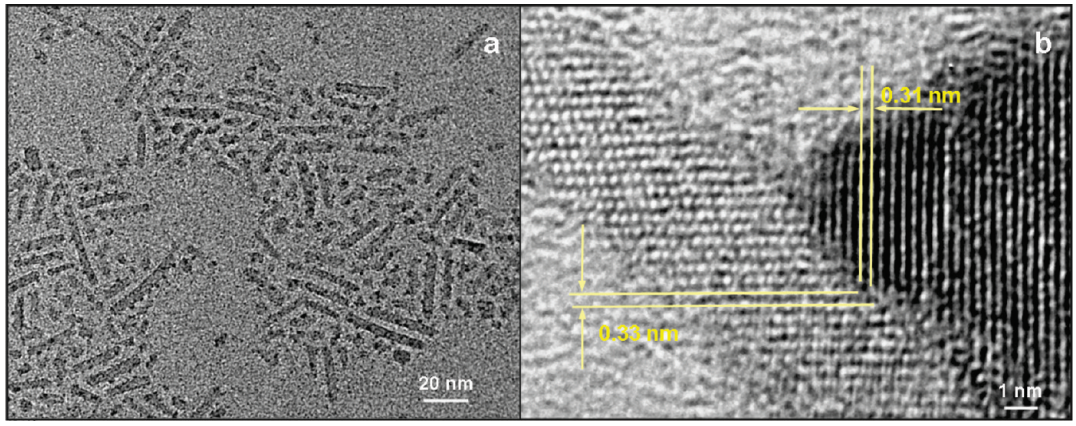


**Figure 3.** (a) Low-magnification transmission electron microscopy (TEM) image of PbSe/$TiO_2$ HNCs. (b). High-resolution TEM image of the PbSe/$TiO_2$ interface, showing quasimatching of crystal lattices along the 110 and 010 faces of PbSe and $TiO_2$, respectively.

was performed according to a method adapted from ref 32 by heating $TiCl_4$ to 300 °C in the presence of OA and OLAM. This approach makes use of a high concentration of Ti precursor in the reaction mixture to yield high-aspect ratio anatase nanorods elongated along the ⟨001⟩ crystallographic direction. Upon formation of $TiO_2$ NRs, the temperature of the reaction mixture was lowered to 180 °C for the growth of PbSe NCs. Typically, a single injection of Pb and Se precursors leads to the formation of 2−3 nm PbSe islands on the surface of nanorods. A small amount of isolated PbSe NCs (<10% of nanoparticles) was also observed in as-prepared reaction mixture and was subsequently reduced to less than 2% after the purification stage (Figure 3a). Additional injections of precursors were needed to fuel the growth of PbSe islands beyond 3 nm in size.

Transmission electron microscopy (TEM) analysis of PbSe/$TiO_2$ HNCs reveals a qualitative difference between the shapes of PbSe NCs forming on the surface of $TiO_2$ NRs as a result of single and multiple injections of Pb and Se precursors. The initial injection leads to the formation of several small-diameter PbSe sites per single NR (Figures 2b,c), with an average site diameter of 1.8−3.0 nm and size dispersion of 10−14% (see Figure S1 for the statistical distribution of diameters). We estimate that the number of PbSe NCs per single $TiO_2$ NR is 21 ± 6, where the dispersion in the number of dots is mainly determined by the dispersion of NR surface areas.

Doubling the concentration of precursors for the first injection was found to produce a 10−15% increase in the density of PbSe dots on the surface of $TiO_2$, but did not affect an average dot size. According to a high-resolution TEM image of a typical PbSe/$TiO_2$ HNC in Figure 2c, PbSe dots appear to be uniformly scattered over the entire NR surface and exhibit a moderate dispersion of sizes. A near-symmetric placement of PbSe dots on the surface of $TiO_2$ can be explained in terms of fundamental energy requirements on the deposition of secondary material in heteroepitaxial growth. Namely, spatially isotropic addition of PbSe monomers onto $TiO_2$ NRs initially results in the formation of a thin PbSe shell. Subsequent lateral expansion of the shell is associated with the mismatch-induced increase of

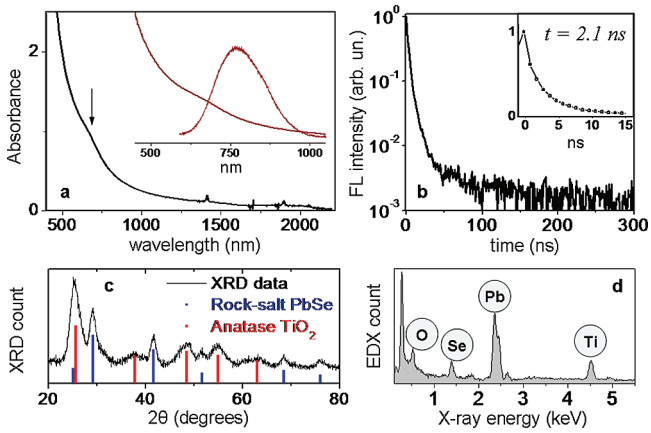


**Figure 4.** Absorption and emission spectra (a) and FL lifetime measurements (b) of PbSe/$TiO_2$ HNCs, comprising 1.9 nm PbSe NCs. X-ray powder diffraction (c) and EDX (d) spectra of PbSe/$TiO_2$ HNCs comprising 4.8 nm PbSe NCs.

the interfacial energy, which promotes the collapse of the PbSe layer into segregated islands.

Secondary injections of precursors were used to induce the growth of larger PbSe NCs on $TiO_2$ surfaces, (Figure 2d,e). The amount of PbSe sites per single NR in this case is reduced to 1 (Figure 2e) or 2 (Figure S2a), which indicates that some of the smaller islands can coalesce into bigger nanoparticles, as evident in the transitional heterostructure (Figure S2a). Such transformation is thermodynamically favorable since the combined surface area of PbSe NCs is reduced during aggregation, causing the reduction in the total surface energy of the heterostructure. A high-resolution TEM image of a PbSe/$TiO_2$ HNC comprising a single 5 nm PbSe NC (Figure 2e) confirms that the surface of a NR is virtually free of small PbSe sites, which supports the coalescence-induced formation of large PbSe NCs. For these structures the volume of the PbSe crystal phase is approximately equal to that of $TiO_2$, as can be deduced form near-equal amplitudes of elemental peaks in EDX spectra (Figure 4d).

Optical properties of PbSe/$TiO_2$ HNCs incorporating 1.9 nm PbSe NCs are analyzed in Figure 4. The absorption profile of PbSe/$TiO_2$ is characteristic of type II heterostructures with nonzero photon absorption in the spectral range below the band gap of both PbSe and $TiO_2$ materials. This is expected because of excitations of intermediate states that exist at the junction of both materials.[33] The highest in energy excitonic feature, corresponding to the band edge absorption in PbSe NCs, can also be identified near 700 nm. Its spectral position correlates well[34] with an estimation from a TEM average PbSe size of 1.9 nm (Figure S1).

As-prepared PbSe/$TiO_2$ HNCs, comprising small-diameter PbSe NCs, show a weak emission feature (emission quantum yield <0.5%) in the 650−900 nm range, as shown in Figure 4a. Both the position and the width of the FL peak are consistent with the expected 1S(e)−1S(h) recombination of carriers in 1.9 nm PbSe NCs, implicating the band-edge origin of the emission.[34] Surprisingly, the contribution of trap states into the FL signal, expected because of a large surface area of PbSe NCs and the possible formation of electron-trapping defects along the strained interface of PbSe and $TiO_2$ domains, was not significant, as evident by the lack of emission originating from below PbSe band gap.

The dynamics of carrier decay was further investigated using FL lifetime measurements (Figure 4b). The observed emission lifetime of 2.1 ns is substantially shorter than expected for 1S(e)−1S(h) excitons in PbSe NCs, for which room-temperature values in excess of 500 ns were reported.[35] We also note that, for small-diameter PbSe NCs, FL lifetimes are expected to increase because of the inverse correlation of the radiative rate and NC band gap.[36] In general, there are two main factors that can potentially lead to such a dramatic decrease of FL lifetimes in PbSe/$TiO_2$ HNCs: electron trapping at defects and oxidation of PbSe NCs via carrier transfer to $TiO_2$. As mentioned above, the signature of trap states emission was not observed in the FL spectra. Likewise, the FL relaxation trend is not typical of carrier traps that generally contribute a long-lived component with decay constants in excess of 1 $\mu$s. Therefore, the observed rapid quenching of FL is attributed to the transfer of photoinduced electrons from PbSe NCs to $TiO_2$ NRs. On the basis of the observed excited-state lifetime, we conclude that the characteristic time scale for photoinduced electron transfer is 2.1 ns, which is significantly faster than 100 ns electron-transfer times observed for organically linked PbS−$TiO_2$ systems.[23]

In summary, we report on a solution-phase synthesis of PbSe/$TiO_2$ heterostructures, comprising small-diameter PbSe nanocrystals grown on the surface of $TiO_2$ nanorods. Fabricated materials exhibit an efficient conversion of visible light energy via a rapid transfer of photoinduced electrons into $TiO_2$ domains. From the general prospective, the present synthesis demonstrates an all-inorganic modification of $TiO_2$ surfaces with semiconductor NCs and could be extended to other nanocrystalline systems, as shown in the Supporting Information for PbS-sensitized $TiO_2$ NRs. Moreover, the heteroepitaxial growth of lead chalcogenides is not limited to $TiO_2$ NRs and can be adapted to other nanostructured forms of $TiO_2$ including porous films and nanotubes, whereby introducing a colloidal route to sensitization of $TiO_2$ surfaces without organic-molecular bridging.

**Acknowledgment.** We gratefully acknowledge Bowling Green State University for financial support (SF07, RIC08, RCE08).

**Supporting Information Available:** Statistical distributions of PbSe diameters, synthesis of PbS/$TiO_2$ heterostructures, and additional TEM images. This material is available free of charge via the Internet at http://pubs.acs.org.

## References and Notes

(1) Linsebigler, A. L.; Lu, G. Q.; Yates, J. T. *Chem. Rev.* **1995**, *95*, 735.
(2) Oregan, B.; Grätzel, M. *Nature* **1991**, *353*, 737.
(3) Augustynski, J. *Electrochim. Acta* **1993**, *38*, 43.
(4) Kay, A.; Grätzel, M. *J. Phys. Chem.* **1993**, *97*, 6272.
(5) Gerischer, H.; Luebke, M. *J. Electroanal. Chem.* **1986**, *204*, 225.
(6) Robel, I.; Subramanian, V.; Kuno, M.; Kamat, P. V. *J. Am. Chem. Soc.* **2006**, *128*, 2385.
(7) Sasha, G.; Gary, H. *J. Phys. Chem.* **1994**, *98*, 5338.
(8) Niitsoo, O.; Sarkar, S. K.; Pejoux, C.; Ruhle, S.; Cahen, D.; Hodes, G. *J. Photochem. Photobiol., A* **2006**, *181*, 306.
(9) Hao, E.; Yang, B.; Zhang, J.; Zhang, X.; Sun, J.; Shen, J. *J. Mater. Chem.* **1999**, *8*, 1327.
(10) Fang, J. J.; Wu, J. X.; Lu, X.; Shen, Y.; Lu, Z. *Chem. Phys. Lett.* **1997**, *270*, 145.
(11) Wijayantha, K. G. U.; Peter, L. M.; Otley, L. C. *Sol. Energy Mater. Sol. Cell.* **2004**, *83*, 363.
(12) Mora-Sero, I.; Bisquert, J.; Dittrich, T.; Belaidi, A.; Susha, A. S.; Rogach, A. L. *J. Phys. Chem. C* **2007**, *111*, 14889.
(13) Lee, J. C.; Sung, Y. M.; Kim, T. G.; Choi, H. J. *Appl. Phys. Lett.* **2007**, *91*, 113104.
(14) Prabakar, K.; Takahashi, T.; Nakashima, T.; Kubota, Y.; Fujishima, A. *J. Vac. Sci. Technol. A* **2006**, *24*, 1613.
(15) Lopez-Luke, T.; Wolcott, A.; Xu, L. P.; Chen, S. W.; Wcn, Z. H.; Li, J. H.; De La Rosa, E.; Zhang, J. Z. *J. Phys. Chem. C* **2008**, *112*, 1282.
(16) Yu, P. R.; Zhu, K.; Norman, A. G.; Ferrere, S.; Frank, A. J.; Nozik, A. J. *J. Phys. Chem. B* **2006**, *110*, 25451.

(17) Vogel, R.; Hoyer, P.; Weller, H. *J. Phys. Chem.* **1994**, *98*, 3183.
(18) Hoyer, P.; Konenkamp, R. *Appl. Phys. Lett.* **1995**, *66*, 349.
(19) Plass, R.; Pelet, S.; Krueger, J.; Gratzel, M.; Bach, U. *J. Phys. Chem. B* **2002**, *106*, 7578.
(20) Nozik, A. *J. Phys. E* **2002**, *14*, 115.
(21) Yu, P. R.; Zhu, K.; Norman, A. G.; Ferrere, S.; Frank, A. J.; Nozik, A. J. *J. Phys. Chem. B* **2006**, *110*, 25451.
(22) Wang, C.; Kwon, K. W.; Odlyzko, M. L.; Lee, B. H.; Shim, M. *J. Phys. Chem. C* **2007**, *111*, 11734.
(23) Hyun, B. R.; Zhong, Y. W.; Bartnik, A. C.; Sun, L.; Abruña, H. D.; Wise, F. W.; Goodreau, J. D.; Matthews, J. R.; Leslie, T. M.; Borrelli, N. F. *ACS Nano* **2008**, *2*, 2206.
(24) Baker, D. R.; Kamat, P. V. *Adv. Funct. Mater.* **2009**, *19*, 805.
(25) Niitsoo, O.; Sarkar, S. K.; Pejoux, C.; Ruhle, S.; Cahen, D.; Hodes, G. *J. Photochem. Photobiol., A* **2006**, *181*, 306.
(26) Das, K.; De, S. K. *J. Phys. Chem. C* **2009**, *113*, 3494.
(27) Markov, I. V. *Crystal Growth for Beginners: Fundamentals of Nucleation, Crystal Growth, and Epitaxy*; World Scientific: Singapore, Malaysia, 2003.
(28) Moreels, I.; Lambert, K.; Muynck, D. D.; Vanhaecke, F.; Poelman, D.; Martins, J. C.; Allan, G.; Zeger, H. *Chem. Mater.* **2007**, *19*, 6101.
(29) Klimov, V.; Hunsche, S.; Kurz, H. *Phys. Rev. B* **1994**, *50*, 8110–8113.
(30) Wehrenberg, B. L.; Guyot-Sionnest, P. *J. Am. Chem. Soc.* **2003**, *125*, 7806.
(31) Wei, S. H.; Zunger, A. *Phys. Rev B* **1997**, *55*, 13605.
(32) Seo, J.; Jun, Y.; Ko, S.; Cheon, J. *J. Phys. Chem. B* **2005**, *109*, 5389.
(33) Hewa-Kasakarage, N. N.; Kirsanova, M.; Nemchinov, A.; Schmall, N.; El-Khoury, P. Z.; Tarnovsky, A. N.; Zamkov, M. *J. Am. Chem. Soc.* **2009**, *131*, 1328.
(34) Evans, C. M.; Gou, L.; Peterson, J. J.; Maccagnano, S.; Krauss, T. D. *Nano Lett.* **2008**, *8*, 2896.
(35) Du, H.; Chen, C.; Krishnan, R.; Krauss, T. D.; Harbold, J. M.; Wise, F. W.; Thomas, M. G.; Silcox, J. *Nano Lett.* **2002**, *2*, 1321.
(36) An, J. M.; Franceschetti, A.; Zunger, A. *Nano Lett.* **2007**, *7*, 2129.

JP907321H